Enhancement of ferromagnetic correlations on multiferroic $TbMnO_3$ by replacing Mn with Co.

V. Cuartero[1], J. Blasco[2], J. García[2], S. Lafuerza[2], G. Subías[2], J. A. Rodriguez-Velamazán[2,3] and C. Ritter[3]

[1] *ALBA Synchrotron/CELLS, Cerdanyola del Vallès, 08290, Spain*
[2] *Instituto de Ciencia de Materiales de Aragón, Departamento de Física de la Materia Condensada,CSIC-Universidad de Zaragoza, Zaragoza, 50009, Spain*
[3] *Institut Laue-Langevin, Boîte Postale 156, 38042 Grenoble Cèdex 9, France*

Abstract. Structural, electronic and magnetic properties of $TbMn_{1-x}Co_xO_3$ ($0.1 \leq x \leq 0.9$) compounds are reported. Samples are isostructural to $TbMnO_3$ adopting the orthorhombic distorted perovskite (*Pbnm*), except for x=0.4, 0.5 and 0.6, where an ordered double perovskite structure ($P2_1/n$) is found. X-ray absorption spectra at the Mn and Co K-edges show an incomplete charge transfer between Mn and Co atoms yielding a mixed valence state Mn^{3+}/Mn^{4+} and Co^{3+}/Co^{2+} for the whole series. Neutron powder diffraction measurements show the development of a ferromagnetic ground state for the intermediate compositions ($0.3 \leq x \leq 0.6$) indicating that the ferromagnetic superexchange Mn^{4+}-O-Co^{2+} interaction is the strongest among a wide set of competitive interactions. The ferromagnetic ordering is, however, not fully achieved and coexists with glassy magnetic properties. With increasing concentration of Co ($x \geq 0.7$) the long range ordering vanishes and only a glassy magnetic behavior with slow dynamics is found. These properties could be related to the existence of magnetically inhomogeneous small clusters arising from competitive magnetic interactions.

1. Introduction.

Multiferroic properties of $TbMnO_3$ have been widely studied since they were discovered in the last decade.[1,2] The multiferroic state appears below $T_{N2}= T_{FE}=27$ K as the Mn sublattice orders in a non-collinear cycloidal magnetic structure which breaks the spatial inversion symmetry allowing ferroelectricity.[1] However, the first magnetic transition in $TbMnO_3$ takes place at $T_{N1}=41$ K, when the Mn sublattice orders in a sinusoidally modulated antiferromagnetic (AFM) structure.[3] We have substituted the Mn sublattice with a magnetic atom, such as Co, in order to perturb the magnetic correlations by creating competing magnetic interactions in $TbMnO_3$.

Co is a trivalent ion in Co-Rare Earth mixed oxides with perovskite structure, showing an electronic configuration $3d^6$ in an octahedral local environment. These compounds exhibit a large variety of properties due to the comparable values of crystal field and intra-atomic exchange energies which give rise to the ability of Co^{3+} ions to adopt different spin states as a function either of temperature or composition.[4,5] Therefore, Co^{3+} can exhibit different electronic configurations depending on the occupation of t_{2g} and e_g orbitals. The configurations for high spin (HS), intermediate spin (IS) and low spin (LS) are $t^4_{2g}\ e^2_g$ (S=2), $t^5_{2g}\ e^1_g$ (S=1) and $t^6_{2g}\ e^0_g$ (S=0)

respectively. Pioneering work on the $LaMn_{1-x}Co_xO_3$ series revealed the existence of a ferromagnetic (FM) ground state in some compositions which was ascribed to FM Mn^{3+}-O-Mn^{3+} correlations.[6] However, later studies point to an evolution of the oxidation state of Mn and Co along the series, from Mn^{3+}-Co^{3+} pairs to Mn^{4+}-Co^{2+} pairs, giving rise to FM superexchange interactions through oxygen ions.[7,8] This result is supported by x-ray absorption studies on $LaMn_{0.85}Co_{0.15}O_3$ showing that Mn dilution by Co favors a 2+ oxidation state for Co and an intermediate valence state for Mn.[9] In related $RMn_{1-x}Co_xO_3$ (R=Rare Earth) compounds, an ordering of the Mn-Co sublattice following the NaCl-structure yields a double perovskite with FM interactions between Co^{2+} and Mn^{4+} ions.[10,11] These results are similar to the properties observed in related $LaMn_{1-x}Ni_xO_3$ series where a double perovskite with a FM ground state is observed for x=0.5 due to the ordering of Mn^{4+} and Ni^{2+} cations.[12]

The appearance of Co^{2+} and Mn^{4+} in $RMn_{1-x}Co_xO_3$ compounds can lead to a large variety of new magnetic interactions. In this way, Co^{2+} with an electronic configuration $3d^7$ is a magnetic ion in both HS (S=3/2) and LS (S=1/2) configurations while Mn^{3+} with electronic configuration $3d^4$ usually adopts the HS configuration (S=2) and Mn^{4+} is also magnetic ($3d^3$, S=3/2). The Goodenough-Kanamori rules[13] for interactions at 180º predict the superexchange interactions indicated in table I. In addition to this large variety of interactions, FM double exchange interaction[14] may also be present in the Mn^{4+}-O-Mn^{3+} pair.

Taking into account the interesting variety of structural and electronic effects and the competing magnetic interactions that can appear along the $TbMn_{1-x}Co_xO_3$ series, this thorough study was undertaken in order to ascertain the structural details and the magnetic ground state of these compounds.

2. Experimental Section.

The powdered samples were synthesized by ceramic methods. First, stoichiometric amounts of Tb_4O_7, $MnCO_3$ and Co_3O_4 are mixed and heated at 1000 ºC for 12 h in air. The resulting powder is pressed into pellets and sintered at 1200 ºC for 24 h in air. Finally, the pellets are repressed and sintered at 1400 ºC for 48 h. The atmosphere used on the last step depends on the Mn/Co rate in order to ensure the appropriate oxygen content and the lack of vacancies. Thus, we used Ar atmosphere for x=0.1, 0.2 and air in the case of x=0.3, 0.4. For Co concentrations $x \geq 0.5$ we used O_2 atmosphere. The oxygen content was tested by cerimetric titration and all samples have the correct oxygen content within experimental error (±0.01).

A preliminary study of the crystallographic structure has been performed by means of x-ray powder diffraction at room temperature, using a Rigaku D/max-B diffractometer with a rotating anode, selecting the Cu K_α wavelength (λ=1.5418 Å). Neutron diffraction experiments have been performed at room temperature at the high intensity D1B (λ=2.52 Å) and high resolution D2B (λ=1.59 Å) instruments at the ILL

(Grenoble, France), in order to properly determine the crystallographic structure of all samples. We have measured the whole series at D1B, and x=0.1, 0.3 and 0.5 samples at D2B. Neutron diffraction patterns have also been collected on D1B as a function of temperature (2 K < T < 200 K) in order to study any long range magnetic ordering at low temperatures.

X-ray absorption experiments have been carried out at the BM25-Spline beam line, at the ESRF (Grenoble, France). We measured both at the Mn and Co K-edge using a double crystal Si (111) monochromator. The energy resolution is $\Delta E/E \sim 10^{-4}$. All spectra were measured in transmission detection mode, at room temperature, using ionization chambers as detectors, so that we have been able to measure up to x=0.6 and x=0.3 Co concentrations at Mn and Co K edge respectively.

A commercial squid magnetometer (MPMS-5s, Quantum Design) was used to determine the macroscopic magnetic properties of the samples between 5 and 300 K, at 0.5 T. Ac susceptibility measurements were carried out at several frequencies and a magnetic field of h_0=4 Oe.

3. Experimental Results.

3.1.Structural and Electronic Properties.

X-ray diffraction patterns show all samples to be single-phase. Rietveld refinements using the Fullprof package[15] are successful using a simple distorted perovskite model (formal ABO_3; A=Tb, B=Mn,Co) with orthorhombic space group *Pbnm.* However, due to the rather different oxidation states of Mn and Co ions, as shown below, it had been expected to find possibly for some values of x an ordered double perovskite structure (formal $A_2BB'O_6$) with monoclinic space group $P2_1/n$, as already found in related compounds.[10,11] This ordered model was therefore as well used to refine the x-ray diffraction patterns, leading, however, to similar results due to the similar atomic numbers of Mn and Co atoms. On the other hand, the neutron scattering lengths of Mn and Co are not only different but have as well different signs giving the possibility to easily recognize an ordered array of both cations using neutron diffraction techniques. Nevertheless, the better angular resolution of the x-ray diffractometer provides an ideal tool to probe the effects of Co substitution on the lattice parameters. Figure 1 shows the evolution of these parameters at room temperature for the whole series, including the parent compound $TbMnO_3$.[16] The three axes present different behaviors: The *a*-axis slightly decreases with increasing Co content with an increased decay starting from x = 0.5. The *b*-axis shows instead first a strong contraction for low x-values and while the shrinkage decreases from x = 0.4. The *c*-axis is the only one exhibiting an expansion with increasing substitution but after reaching a maximum expansion for x~0.4-0.5 it also contracts for higher values of x. Overall, the unit cell volume shrinks with increasing Co content with an inflection point around x=0.5. This central region corresponds to the monoclinic samples with an ordered array of Mn and Co as shown from the neutron patterns below.

Neutron patterns collected at D1B for the whole series reveal a significant difference for samples around x=0.5: The existence of the (0 1 1) reflection which is forbidden in the *Pbnm* space group. This agrees with an ordered array of Mn and Co atoms on the perovskite B-site reducing the cell symmetry to $P2_1/n$. Unfortunately, the high neutron flux of D1B setup presents a small $\lambda/2$ contamination (≈0.6%) yielding the harmonic of (0 2 2) reflection at the same *d*-spacing of the mentioned (0 1 1) reflection. For samples with $0.4 \leq x \leq 0.6$ the best refinements were obtained using the monoclinic cell while for the rest of the compositions there were not significant differences between both possibilities suggesting the lack of Mn-Co ordering. In order to assure this point, we performed measurements on x=0.1, 0.3 and 0.5 at D2B (λ=1.59 Å) giving patterns with higher angular resolution and free of any harmonic contamination. The best refinements are summarized in table II and we represent in Fig. 2 the Rietveld refinement for two representative samples (x=0.3 and 0.5). These results confirmed our previous analysis with D1B data. The lack of (0 1 1) reflection confirms that x=0.3 sample is a simple perovskite whereas a weak peak in the x=0.5 pattern can only accounted for by a monoclinic cell. The best refinement yields a double perovskite with two crystallographic sites for the perovskite B-site and a concentration of 25.5±1% of *anti-site* defects, i.e. miss-placed atoms (B atoms at B' position and *vice versa*, 50% means simple perovskite).

Table II shows the structural parameters derived from these refinements for x=0.1, 0.3 and 0.5. The most significant change is related to the bond lengths. $TbMn_{0.9}Co_{0.1}O_3$ shows a distorted BO_6 octahedron with a *zig-zag* sequence of long and short B-O distances in the *ab*-plane. The substitution of Mn by Co decreases this distortion, the longest B-O bond length decreases and the overall BO_6 octahedra tend to be more regular. This is related to the decrease in the difference between *a*- and *b*- lattice parameters (see Fig. 1). We have used the bond valence analysis to calculate the oxidation state of Mn and Co from their bond lengths using the Zachariasen formula.[17] In $TbMn_{0.9}Co_{0.1}O_3$, the B-O distances agree with oxidation states of $Mn^{+3.05}$ and $Co^{+2.2}$, therefore, there is no stress in the lattice associated to placing a Mn^{3+} cation inside this BO_6 octahedron but a Co^{3+} seems to be under-bonded. In the case of $TbMn_{0.7}Co_{0.3}O_3$, the refined bond lengths yield oxidation states of +3.1 and +2.2 for Mn and Co ions. The Co continues to be under-bonded while Mn starts to be over-bonded. Finally, there are two BO_6 octahedra in the $TbMn_{0.5}Co_{0.5}O_3$ sample corresponding to the two Wyckoff positions, *2d* and *2c*, available for Mn and Co. The BO_6 octahedron (*2d*) with a volume of around 11.32 $Å^3$ is composed of ~75% Co atoms and 25% Mn ones. The ionic bond valence model yields $Co^{+2.3}$ and $Mn^{+2.8}$. The B'O_6 octahedron (*2c*) has a volume of 9.82 $Å^3$ with the opposite atom composition and the calculated valences are $Co^{+3.0}$ and $Mn^{+3.6}$. As a first approximation, B and B' sites favor the existence of Co^{2+} and Mn^{4+} cations respectively, while misplaced atoms might be favored in the trivalent state.

In order to gain insights into the atom valences, x-ray absorption near edge spectroscopy (XANES) was used. Figure 3 shows all XANES spectra measured in transmission. We show the spectra of the x=0, 0.1, 0.3, 0.4, 0.5 and 0.6 samples at the

Mn K edge (upper panel) and down to x=0.3 at the Co K edge (lower panel). The Athena module (version 0.8.058) of IFEFFIT package[18] has been used for background subtraction and normalization of all spectra. In both cases, there is a shift of the edge to higher energies as the Co content increases, so we expect the oxidation state of Mn and Co to increase along the series. In order to properly set the oxidation state of the transition metal (TM) ions, we will take into account the empirical linear relation between the chemical shift of the edge and the valence state of the absorbing atom.[19] In particular, in the case of Mn^{3+} and Mn^{4+} ions showing octahedral local structure, the chemical shift is around 4.2 eV,[20] while it is 3.5 eV in the case of Co^{2+} and Co^{3+} in an octahedral coordination.[21] Here, we will consider $TbMnO_3$ and $TbCoO_3$ as reference compounds for Mn^{3+} and for Co^{3+} respectively. The variation of the chemical shift in the Mn K edge is not continuous with the composition. We find the maximum chemical shift for x=0.5 and 0.6 range, without achieving the edge position of $CaMnO_3$ (Mn^{4+}). Therefore, as Mn is substituted by Co, Mn appears as a Mn^{3+}/Mn^{4+} mixed valence state, as it happens in $La_{1-x}Ca_xMnO_3$.[20] In the case of the Co K edge (lower panel Fig. 3), there is also a chemical shift of the edge to higher energies with increasing x-value, associated with the evolution of the Co oxidation state from ~2.4+ up to 3+ for $TbCoO_3$.

The valence inferred from the chemical shift of both edges is plotted in the Figure 4. The valence of Mn increases with increasing Co content up to reach a value of +3.6 for x=0.5 and x=0.6. Conversely, the valence of Co decreases with increasing the Mn content from 3 (x=1) down to 2.4 (x=0.5). So, definitely there is a charge redistribution along the whole $TbMn_{1-x}Co_xO_3$ series but the '*formal equilibrium*' $Mn^{3+}+Co^{3+} \leftrightharpoons Mn^{4+}+Co^{2+}$ is not completely shifted to the right, giving rise to a mixed valence state Mn^{3+}/Mn^{4+} and Co^{3+}/Co^{2+}, as it happens in the $LaMn_{1-x}Co_xO_3$ series.[21] This result is in agreement with the evolution of B-O distances obtained from the refinements of neutron powder diffraction patterns (table II) and it may be related to the existence of *anti site* defects in the double perovskite compounds.

Furthermore, this result is also in agreement with the evolution of the peaks at the pre-edge region of the Co K edge. These are related to transitions from the 1s orbitals to 3d TM orbitals hybridized with 2p oxygen orbitals.[22] The intensity of the prepeak increases as Co increases its oxidation state, which is in also in agreement with an increase of the Co-O covalency as the Co valence tends to 3.

3.2.Magnetic properties.

All samples show a paramagnetic behavior at room temperature. Effective paramagnetic moments have been determined by fitting the inverse of the magnetic DC susceptibility to the Curie-Weiss law at high temperatures, as shown in figure 5 for x=0.1, 0.3, 0.5 and 0.9. The best fit parameters are collected in table III. Overall, both the Curie constant and the effective paramagnetic moment decrease as the Co content increases. The inset of Fig. 5 represents the effective paramagnetic moments obtained from the fit, together with the theoretical moments (dashed line) that are obtained considering a full disproportion model of the abovementioned formal equilibrium and

the paramagnetic contribution from Tb^{3+}. As a first approximation, it is considered that for x<0.5 the charge disproportion is Mn^{3+}/Mn^{4+} and Co^{2+}, while for x>0.5 it is Mn^{4+} and Co^{3+}/Co^{2+}. For x=0.5, we consider that all magnetic contribution comes from the Mn^{4+}-O-Co^{2+}(HS) interaction. This model gives the theoretical paramagnetic moments included in table III and they correspond to the dashed line in the inset of Fig. 5, which nicely follows the trend of the experimental results. The Weiss constants obtained from the fits also change with the composition. Samples at the edges of the series show negative values while central compositions exhibit positive values. This result indicates the predominance of AFM correlations (Mn^{3+}-O-Mn^{3+} or Co^{3+}-O-Co^{3+}) at the edges while FM interactions (mainly Mn^{4+}-O-Co^{2+}) are greater at intermediate compositions reaching their maximum value for x=0.5.

The evolution of magnetic properties at low temperatures is strongly changing as function of the Co content. These properties were probed by studying the temperature dependence of neutron diffraction patterns between 200 and 2 K and also using macroscopic magnetic measurements. In the case of low doped samples ($x\leq0.2$) we do not appreciate any variation on the neutron patterns down to 2 K. As an example, in figure 6 the thermodiffractogram of $TbMn_{0.9}Co_{0.1}O_3$ is shown, there are no additional AFM peaks appearing at low temperatures pointing to the absence of AFM long range correlations in this sample. It is noteworthy that this small amount of a non-isovalent cation doping (10%) destroys long range magnetic ordering in $TbMnO_3$. This is in contrast to isovalent substitutions with Ga^{3+} or Sc^{3+},[23,24] where Mn^{3+} long range AFM ordering is not totally suppressed with 10% doping. An increase of the intensity is not observed either at any reflection for this sample, which discards FM long range ordering. At low temperatures, we observe a broad bump at low angles, which corresponds to the diffuse scattering ascribed to the ordering of Tb^{3+} moments, which is also observed in other dilutions.[17,18] Compared to undoped $TbMnO_3$ the coherence length of the Tb^{3+} ordering decreases by the dilution of the Mn sublattice.

The results are very different for samples with intermediate Co contents in the range $0.3\leq x\leq0.6$. As can be seen in the right panel of fig 7 for x=0.4 and 0.5 there is an increase of the (110) and (002) nuclear reflections below a certain temperature, which can be related to the appearance of long range FM interactions. No other changes are observed in the thermodiffractograms excluding the appearance of AFM long range correlations. Figure 7 (a) shows the evolution with temperature of the sum of (110) and (002) intensities for this composition range ($0.3\leq x\leq0.6$) and Fig. 7(b) exhibits the ac magnetic susceptibility. The ferromagnetic contribution to the (110) and (002) peaks increases in these samples below the transition temperatures observed in the ac susceptibility curve, which are identified by vertical lines in Fig. 7 (b). The transition temperatures are T_N= 61, 89, 101 and 98 K for x=0.3, 0.4, 0.5 and 0.6 respectively. A stronger increase is observed for x=0.4 and 0.5 reflecting stronger FM long range correlations for these Co concentrations. For x=0.3 and 0.6 only a small increase in the Bragg peak intensities is visible making a full long range ordering involving the whole compound very unlikely. Finally, these neutron patterns keep showing the appearance

of diffuse scattering at very low temperature indicating that the ordering of Tb^{3+} is again only short range in this composition range.

The magnetic structure was refined for samples with $0.4 \leq x \leq 0.6$ from the neutron patterns collected at D1B at low temperature. We have refined an overall magnetic moment for atoms located at 2c and 2d positions testing different orientations for the moments. As a first approximation we have considered the magnetic contribution as originating only from Co atoms at the *2d* position and only from Mn atoms at *2c*. The best refinement was achieved for moments oriented within the *ac*-plane. We tried to refine two different moment values for the two different positions in order to distinguish between Mn and Co contributions but the refinement either diverges or holds with $\mu_{Mn} \approx \mu_{Co}$. This result suggests that Co^{2+} is in its high spin state, so that S=3/2 for both Mn^{4+} and Co^{2+}. This high spin configuration of Co is also observed in other related double perovskites such as Lu_2MnCoO_6.[25] As it is neither possible to discriminate the magnetic moment values on the two TM Wykoff positions nor to determine the exact direction of the magnetic moments within the ac-plane due to the insufficient experimental resolution in this pseudocubic compounds we determined an average value of the magnetic moments for those samples which show a significant increase of the magnetic peaks. The obtained values are 0.6, 1.0 and 0.8 μ_B per transition metal site for $TbMn_{0.6}Co_{0.4}O_3$, Tb_2MnCoO_6 and $TbMn_{0.4}Co_{0.6}O_3$, respectively at T=10 K. The refined moments are significantly smaller than the expected ones for a fully polarized transition metal sublattice. Competing magnetic interactions and *anti-site* defects might account for this decrease. In this way, considering a full charge redistribution (only Mn^{4+} and Co^{2+}), the main superexchange Mn^{4+}-O-Co^{2+}interaction between ions on the correct position is FM but the corresponding interaction between cations misplaced due to *anti-site* defects would be AFM as indicated in table I (Mn^{4+}-O-Mn^{4+} or Co^{2+}-O-Co^{2+}). Within this simple model, an amount of 33% of AS would yield a theoretical magnetic moment of ~1 μ_B per transition metal site for $TbMn_{0.5}Co_{0.5}O_3$. As there is no full charge redistribution in this series (see Fig. 3), the existence of Co^{3+} and Mn^{3+} randomly distributed could give rise to competitive interactions reducing the total FM moment with a smaller amount of AS defects. We would like to recall here that the refinement of the high resolution neutron data of $TbMn_{0.5}Co_{0.5}O_3$ revealed the presence of 25% of *anti-site* defects. Another possibility is that competitive interactions lead to an inhomogeneous disordered magnet with regions that do not participate in the magnetic ordering. In this case a dynamic behavior could be observed in the ac susceptibility curves, we will discuss the frequency shift of the magnetic peak seen for Tb_2MnCoO_6 below.

DC magnetization measurements confirm the neutron diffraction results for the intermediate compositions. Transitions to a magnetic ground state can be seen in figure 8 (a), where the temperature dependences of DC magnetization are shown under zero field (ZFC) and field (FC) cooling conditions. ZFC and FC branches show different thermal behavior below certain irreversibility temperatures, being T_{irr}= 52, 70 and 76 K for x=0.3, 0.4 and 0.6 respectively. The Tb_2MnCoO_6 sample shows a peak at T_{peak}=90

K, and ZFC and FC curves separate at T_{irr}= 84K. This behavior is characteristic of materials with magnetic inhomogeneities showing glassy properties.[26] This might be another indication that a full FM state is not achieved in the whole sample due to competitive interactions.

Higher doped samples such as x=0.7 and 0.8 show a similar macroscopic magnetic behavior to x=0.3 and 0.4 samples. Fig. 8 (b). shows how the ZFC and FC branches separate below T_{irr}~70K for x=0.7 and 0.8. However, the neutron diffraction patterns do not show any significant changes with temperature for these compositions, as shown in the inset of fig. 8 (b) for $TbMn_{0.7}Co_{0.3}O_3$. The broad peak appearing at low temperatures at low angles is again related to the Tb short range ordering. Neutron diffraction patterns for x=0.8 and 0.9 (not shown here) reproduce the results of $TbMn_{0.7}Co_{0.3}O_3$. Thus, for higher doped samples (x=0.7, 0.8 and 0.9), there is no long range magnetic ordering. In the case of $TbMn_{0.1}Co_{0.9}O_3$, there is as well no significant magnetic irreversibility in the DC magnetization curves as can be seen in fig. 8 (b).

In order to further investigate the magnetic behavior of the higher doped samples, we have performed ac susceptibility measurements at different frequencies to probe the glassy properties of $x \geq 0.5$ samples. As displayed in figure 9, all samples show frequency-dependent peaks. The temperature shift is very small and it ranges between 0.2 and 0.4 K for a frequency change of ~1 KHz. The peaks are very sharp and the heights of both, real and imaginary components, decrease with increasing the ac frequency in agreement with a type B spin glass.[27] However our attempts to analyze the dynamic behavior by using either a Vögel-Fulcher law or a power law with a critical exponent[28] were unsuccessful as we obtained very large relaxation times and very small activation energies (or critical exponents) in both cases. However, the appearance of frequency-dependent peaks involving slow spin dynamics has been also observed in inhomogeneous disordered magnets[29] so a plausible scenario would be that competitive interactions develop magnetic clusters of variable size. For the x=0.5 sample, large FM regions contributing to the neutron diffraction patterns coexist with smaller magnetic clusters. With increasing x the FM interactions diminish and the resulting cluster size is smaller than the coherence length observable by neutron diffraction while the glassy behavior as seen in the susceptibility data is preserved.

4. Conclusions.

The $TbMn_{1-x}Co_xO_3$ series has been synthesized for all Co concentrations by conventional ceramic methods. All samples are single phase and their crystallographic structure has been determined by x-ray and neutron diffraction measurements. Low and high doped samples are single distorted perovskite with an orthorhombic cell (space group Pbnm) while intermediate samples ($0.4 \leq x \leq 0.6$) show a double perovskite structure (monoclinic cell with space group $P2_1/n$) with *anti-site* defects.

The valence state of Mn and Co has been determined by x-ray absorption spectroscopy. Mn and Co are trivalent in the parent compounds $TbMnO_3$ and $TbCoO_3$, respectively. A charge redistribution along the whole $TbMn_{1-x}Co_xO_3$ series with an oxidation of Mn^{3+} ions coupled to a reduction of Co^{3+} cations is found. However, the relation $Mn^{3+}+Co^{3+} \leftrightharpoons Mn^{4+}+Co^{2+}$ is not completely shifted to the right, giving rise to a mixed valence state with Mn^{3+}/Mn^{4+} and Co^{3+}/Co^{2+}. This result is in agreement with the evolution of B-O (B=Mn, Co) distances and the decrease with increasing x of the global distortion ascribed to Mn^{3+}. The mixed valence of both atoms also explains the magnetic properties of these compounds. For $x \leq 0.3$ compounds no long range magnetic ordering is found by neutron diffraction. The non-isovalent substitution with Co destroys the AFM orderings of both Mn and Tb moments typical of $TbMnO_3$ already for x=0.1. In the concentration range $0.4 \leq x \leq 0.6$, the structural order of Mn/Co on two different crystallographic sites and the charge redistribution on these ions favor the FM superexchange Mn^{4+}-O-Co^{2+} correlations which are strongest for x=0.5. Long range FM ordering has been found in this concentration range by neutron diffraction but the refined magnetic moment values are below the expected value for a fully polarized metal transition sublattice. The existence of competitive interactions in absence of complete charge redistribution and the existence of structural disorder due to *anti-site* defects could lead to magnetic frustration and glassy properties coexisting with long range magnetic order in these compounds.

Frequency dependent ac susceptibility data reveal for samples with $x \geq 0.7$ glassy magnetic properties with very slow dynamics discarding a canonical spin glass behavior. The weakness of Mn^{4+}-O-Co^{2+} FM correlations in this range favor the disappearance of long range FM clusters and the existence of an inhomogeneous disordered magnet composed of small magnetic clusters.

ACKNOWLEDGEMENTS

The authors thank ESRF and ILL for granting beam time, especially the Spanish CRG BM25, D15 and D1B instruments. Financial support from Spanish MICINN (project FIS08-03951 and MAT2007-61621) and DGA (CAMRADS) is acknowledged.

References.

[1] T. Kimura, T. Goto, H. Shintani, K. Ishizka, T. Arima and Y. Tokura, Nature (London) **426**, 55 (2003).

[2] T. Kimura, G. Lawes, T. Goto, Y. Tokura and A. P. Ramirez, Phys Rev. B **71**, 224425 (2005)

[3] M. Kenzelmann, A. B. Harris, S. Jonas, C. Broholm, J. Schefer, S. B. Kim, C. L. Zhang, S.-W. Cheong, O.P. Vajk and J. W. Lynn, Phys. Rev. Lett. **95**, 087206 (2005).

[4] M. A. Korotin et al. Phys. Rev. B **54**, 5309 (1996).

[5] R. Ibarra et al., Phys Rev. B **57**, R3217 (1998).

[6] J. B. Goodenough, A. Wold, R. J. Arnott, and N. Menyuk, Phys. Rev. **124**, 373 (1961).
[7] G. Blasse, J. Phys. Chem. Solids **26** 1969 (1965).
[8] R. I. Dass and J. B. Goodenough, Phys. Rev. B **67**, 014401 (2003).
[9] J.-H. Park, S.-W. Cheong, C. T. Chen, Phys. Rev. B **55**, 11072 (1997)
[10] I. O. Troyanchuk, L.S. Lobanovsky, D. D. Khalyavin, S. N. Pastushonok, H. Szymczak. J. Magn. Magn. Mat. **210**, 63 (2000).
[11] I. O. Troyanchuk, N. V. Samsonenko, N. V. Kasper, H. Szymczak and A. Nabialek, J. Phys.: Condens. Matter **18** 9541 (1997).
[12] J. Blasco, J. García, M. C. Sánchez, J. Campo, G. Subías, and J. Pérez-Cacho, Eur. Phys. J. B **30**, 469 (2002).
[13] J. B. Goodenough, Phys. Rev. **100**, 564 (1995); J. Kanamori, J. Phys. Chem. Solids **10**, 87 (1959).
[14] C. Zener, Phys. Rev. **82**, 403 (1951).
[15] J. Rodríguez-Carvajal, Physica B **192**, 55 (1993).
[16] J. Blasco, C. Ritter, J. García, J. M. de Teresa, J. Pérez-Cacho, and M. R. Ibarra, Phys. Rev. B **62** 5609 (2000)
[17] N. E. Brese and M. O'Keeffe, Acta Cryst. **B47**, 192 (1991).
[18] M. Newville, J. Synchrotron Rad. **8**, 322 (2001); B. Ravel and M. Newville, *ibid.* **12**, 537 (2005).
[19] J. García, G. Subías, V. Cuartero and J. Herrero-Martín, J. Synchrotron Rad. **17**, 386 (2010).
[20] G. Subías, J. García, M. G. Proietti and J. Blasco, Phys. Rev. B **56**, 8183 (1997).
[21] M. Sikora, Cz. Kapusta, K. Knízek, J. Jirák, C. Autret, M. Borowiec, C. J. Oates, V. Procházka, D. Rybicki and D. Zajac, Phys. Rev. B **73**, 094426 (2006).
[22] S. Lafuerza, G. Subías, J. García, S. Di Matteo, J. Blasco, V. Cuartero and C. R. Natoli, J. Phys.: Condens. Matter **23**, 325601 (2011).
[23] V. Cuartero, J. Blasco, J. García, G. Subías, C. Ritter and J. A. Rodríguez-Velamazán, Phys. Rev. B **81**, 224117 (2010).
[24] O. Prokhnenko, N. Aliouane, R. Feyerherm, E. Dudzik, A. U. B. Wolter, A. Maljuk, K. Kiefer, and D. N. Argyriou, Phys. Rev. B **81**, 024419 (2010).
[25] S. Yáñez-Vilar, E. D. Mun, V. S. Zapf, B. G. Ueland, J. Gardner, J. D. Thompson, J. Singleton, M. Sánchez-Andújar, J. Mira, N. Biskup, M. A. Señarís-Rodríguez, C. D. Batista, Phys, Rev. B **84**, 134427 (2011).
[26] K. De, S. majumdar and S. Giri, J. Phys. D: Appl. Phys. **40**, 5810 (2007).
[27] K. L. Ngai, A. K. Rajagopal an C. Y. Huang, J. Appl. Phys. 55, 1714 (1984).
[28] J. Souletie and J. L. Tholence, Phys. Rev. B **32**, 516 (1992).
[29] R. Mathieu and Y. Tokura, J. Phys. Soc. Jap. **76**, 124706 (2007).

Tables

Table I. Combination table for the expected magnetic superexchange B-O-B' interactions from Goodenough-Kanamori rules (180º) of the possible B (Mn or Co) ions in $TbMn_{1-x}Co_xO_3$ samples. B and B' are ordered in columns and rows and the commutation law holds. AFM and FM stand for antiferromagnetic and ferromagnetic interactions, respectively.

	Mn^{3+}	Mn^{4+}	Co^{2+}	Co^{3+} (LS)	Co^{3+} (IS or HS)
Mn^{3+}	AFM	FM	AFM	FM	AFM
Mn^{4+}	FM	AFM	FM	AFM	FM
Co^{2+}	AFM	FM	AFM	FM	AFM
Co^{3+} (LS)	FM	AFM	FM	AFM	FM
Co^{3+} (IS or HS)	AFM	FM	AFM	FM	AFM

Table II. Structural parameters (space group, lattice parameters, fractional coordinates and isotropic temperature factors), reliability factors and bond lengths and bond angles in BO_6 octahedra obtained from the refinement of neutron diffraction data fromD2B.

	x=0.1	x=0.3	x=0.5
Space Group	Pbnm	Pbnm	$P2_1/n$
a (Å)	5.3133(1)	5.3088(1)	5.2955(1)
b (Å)	5.8027(1)	5.6642(1)	5.5979(1)
c (Å)	7.4633(1)	7.5363(1)	7.5400(1)
β (º)	90	90	89.97(1)
Tb: x	-0.0188(2)	-0.0156(3)	0.0164(2)
y	0.0780(2)	0.0707(3)	0.0679(2)
z	1/4	1/4	0.2480(6)
B_{iso} (Å^2)	0.65(3)	0.21(3)	0.15(2)
Mn/Co: B_{iso} (Å^2)	0.65(4)	0.26(6)	0.19(12)
O1: x	0.1063(3)	0.1008(3)	0.2982(6)
y	0.4657(2)	0.4690(3)	0.3101(5)
z	1/4	1/4	0.0487(5)
B_{iso} (Å^2)	0.96(3)	0.57(4)	0.28(6)
O2: x	0.7014(2)	0.6969(2)	0.3136(6)
y	0.3205(2)	0.3076(3)	0.2931(5)
z	0.0511(2)	0.0510(2)	0.4482(6)
B_{iso} (Å^2)	0.97(3)	0.63(3)	0.57(7)
O3: x	--	--	0.6002(3)
y	--	--	0.9691 (3)
z	--	--	0.4482(6)
B_{iso} (Å^2)	--	--	0.47(3)
R_{Bragg} (%)	3.5	2.8	2.7
□^{2}	1.7	1.5	1.6
<B-O1-B> (º)	144.41(2)	146.71(2)	147.8(1)
<B-O2-B> (º)	145.87(4)	146.88(4)	147.2(1)
<B-O3-B> (º)	--	--	147.0(3)
B-O1 (Å)	1.9596(5)	1.9664(5)	2.071(3)
B-O2 (Å)	2.1758(11)	2.0682(11)	2.040(3)
B-O2/O3 (Å)	1.9387(11)	1.9813(11)	1.988(5)
B´-O1 (Å)	--	--	1.939(3)
B´-O2 (Å)	--	--	1.954(3)
B´-O3 (Å)	--	--	1.944(5)

Table III. Magnetic parameters (Curie and Weiss constants, effective paramagnetic moment) obtained from the fit to a Curie-Weiss law together with the theoretical effective paramagnetic moments from the ionic configuration of transition metal indicated in the last column in addition to the effective paramagnetic moment of Tb^{3+} ($\rho_{Tb}= 9.72\mu_B$).

x	C(emu·K/mol)	θ (K)	ρ_{eff} (μ_B/f.u.)	ρ_{the} (μ_B/f.u.)	Theor. ions
0.1	14.55	-9.6	10.79	10.80	$Mn^{3+}/Mn^{4+}–Co^{2+}$
0.2	15.32	-8.2	11.07	10.72	$Mn^{3+}/Mn^{4+}–Co^{2+}$
0.3	14.66	-1.3	10.80	10.63	$Mn^{3+}/Mn^{4+}–Co^{2+}$
0.4	12.28	12.0	9.96	10.55	$Mn^{3+}/Mn^{4+}–Co^{2+}$
0.5	13.56	30.2	10.42	10.46	$Mn^{4+}–Co^{2+}$
0.6	12.83	19.6	10.19	10.32	$Mn^{4+}–Co^{2+}/Co^{3+}$
0.7	13.27	7.7	10.24	10.17	$Mn^{4+}–Co^{2+}/Co^{3+}$
0.8	12.95	6.2	10.14	10.02	$Mn^{4+}–Co^{2+}/Co^{3+}$
0.9	12.51	-8.5	10.01	9.87	$Mn^{4+}–Co^{2+}/Co^{3+}$

Figures

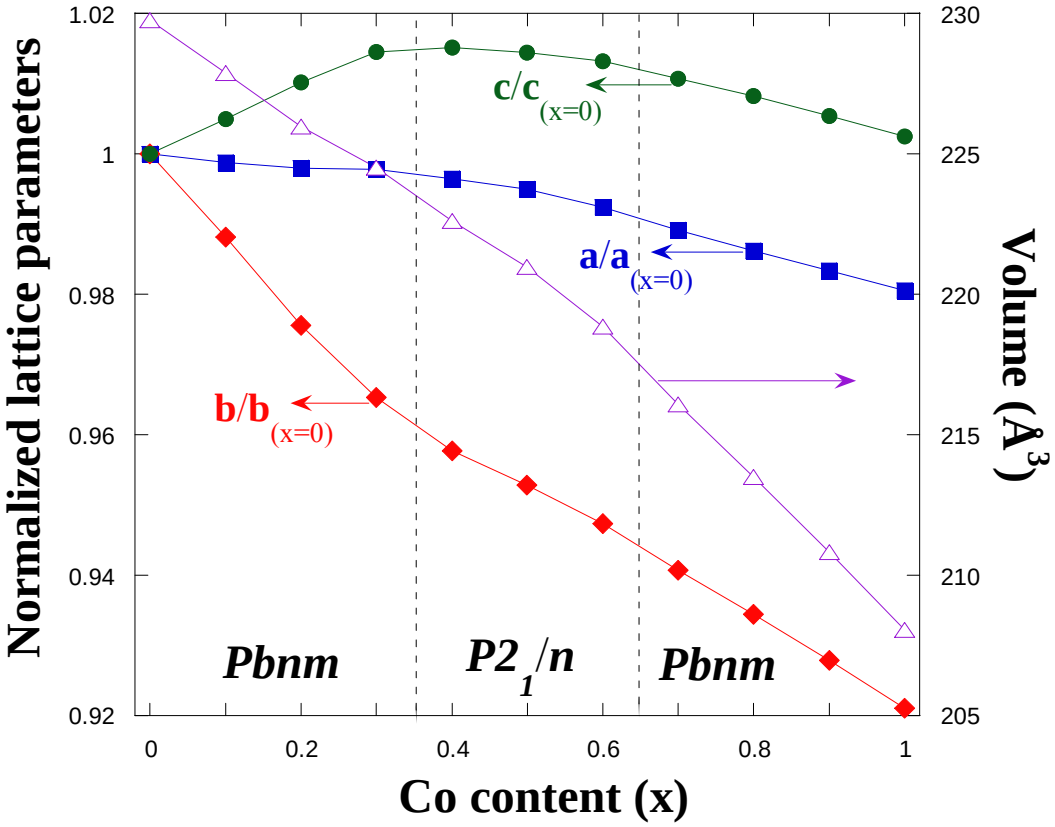

Fig. 1. Composition dependence of the lattice parameters of $TbMn_{1-x}Co_xO_3$ samples. The data have been normalized to the values of $TbMnO_3$ taken from Ref. 16. Dashed lines are guides to the eye to approximately separate regions with simple (*Pbnm*) and double ($P2_1/n$) perovskites.

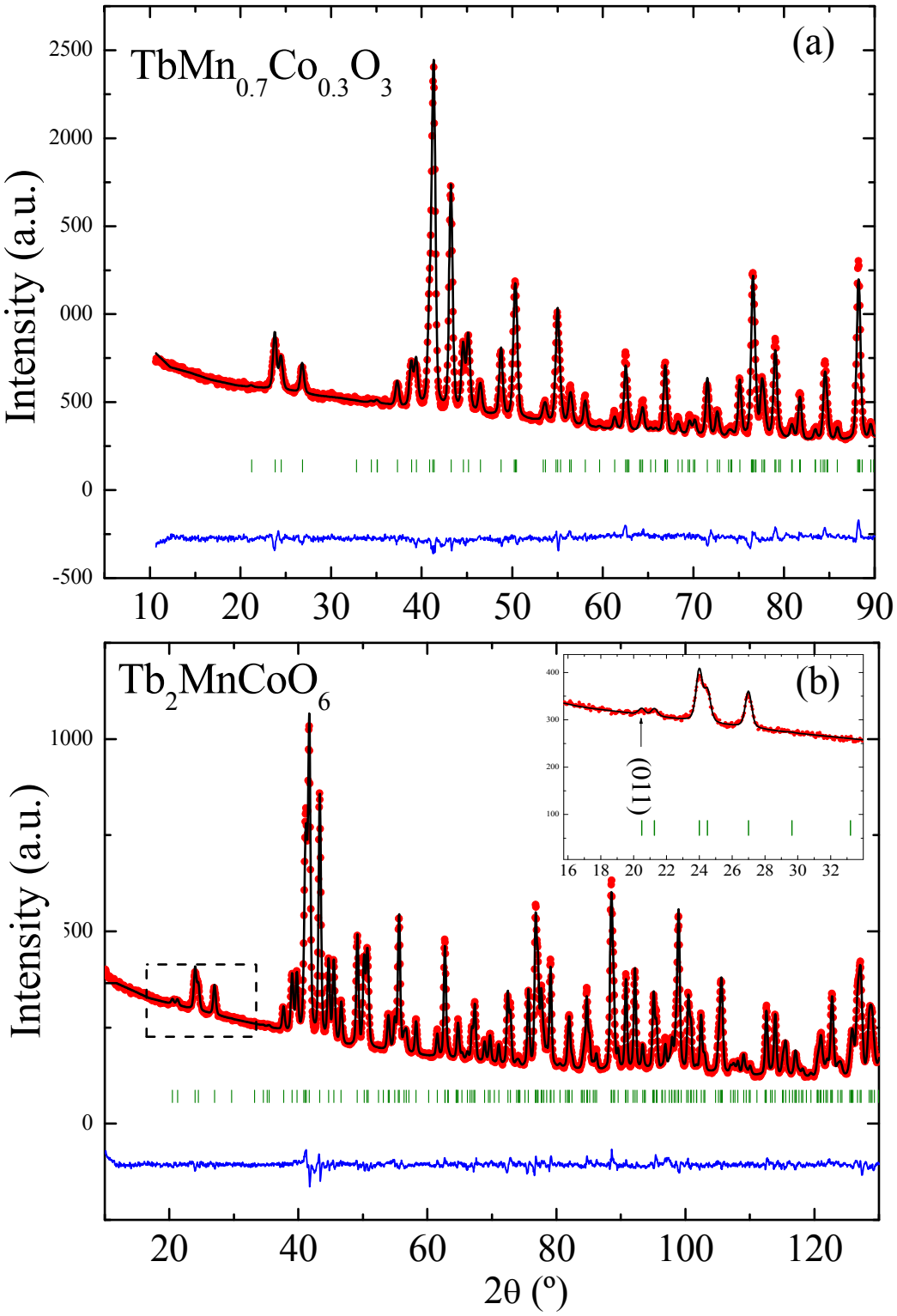

Fig 2. Neutron diffraction patterns of x=0.3 and 0.5 samples, measured at room temperature at D2B. (a) $TbMn_{0.7}Co_{0.3}O_3$ using a simple perovskite model and (b) $TbMn_{0.5}Co_{0.5}O_3$ using a double perovskite model, with 25.5% antisites. Inset: superstructure peak characteristic of a double perovskite crystallographic structure.

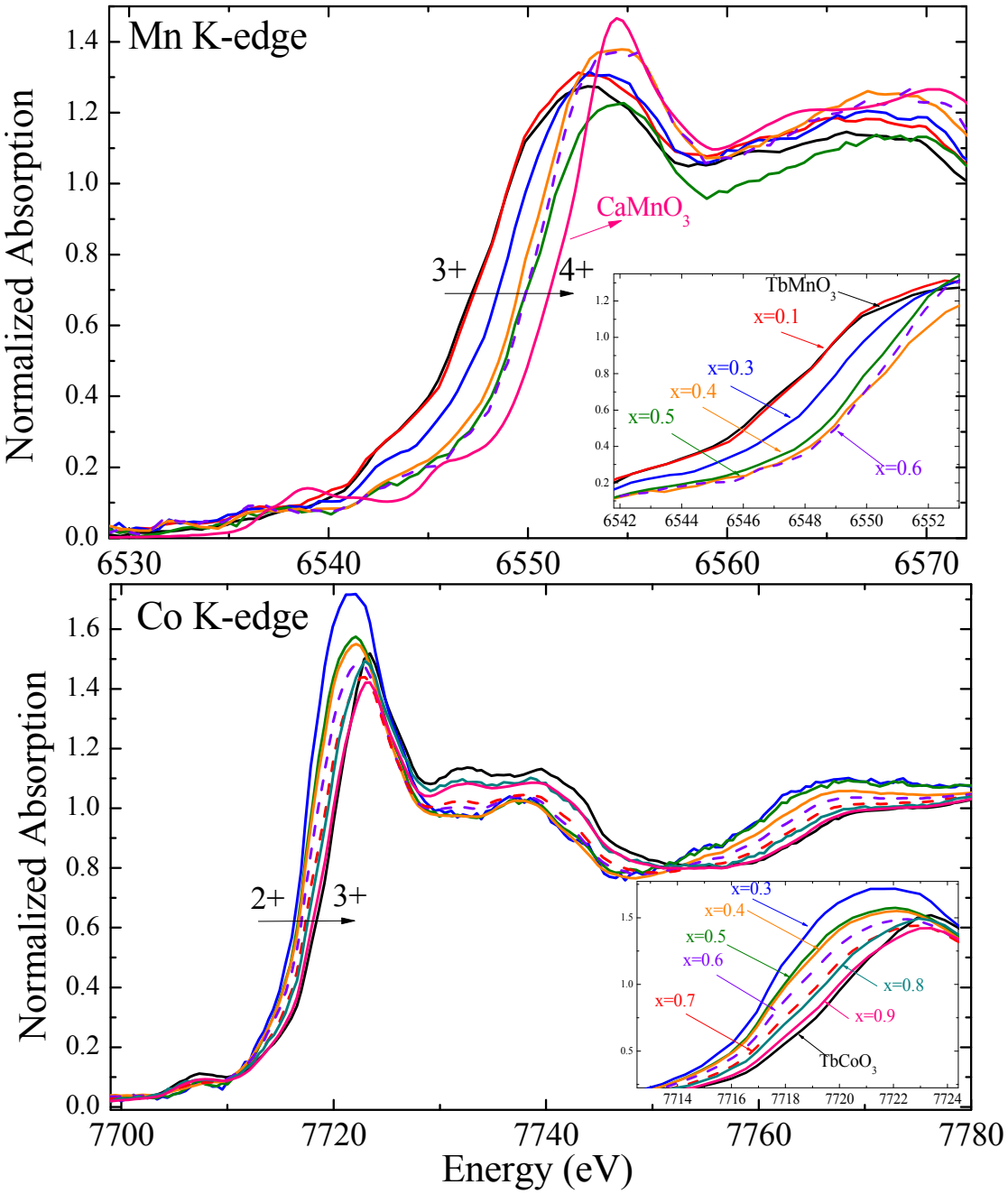

Fig. 3. Normalized x-ray absorption spectra of $TbMn_{1-x}Co_xO_3$ samples at the Mn (upper panel) and Co (lower panel) K edge, measured in transmission. Insets: detail of the edge and white line of the spectra.

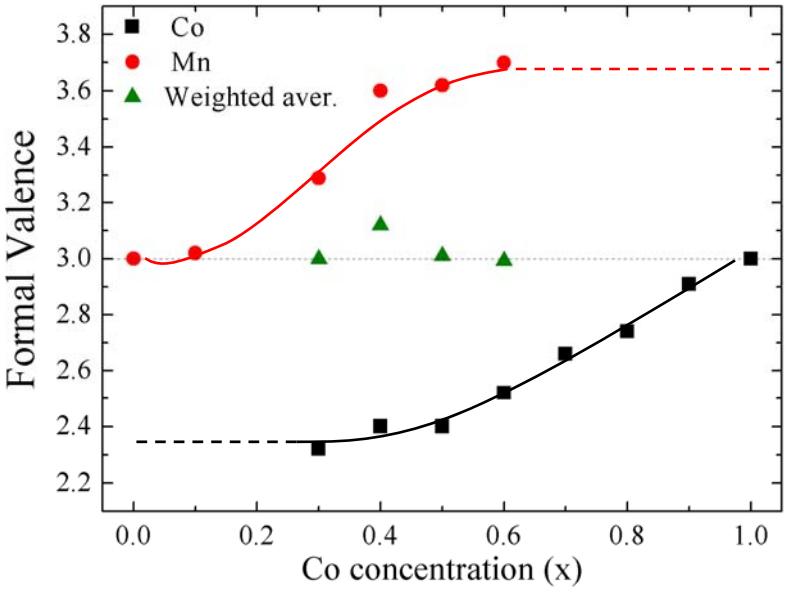

Fig. 4. Evolution of the formal valence of Mn (circles) and Co (squares) along the $TbMn_{1-x}Co_xO_3$ series obtained from the chemical shift of Mn K and Co K edges. Triangles represent the weighted average valences obtained from both atoms.

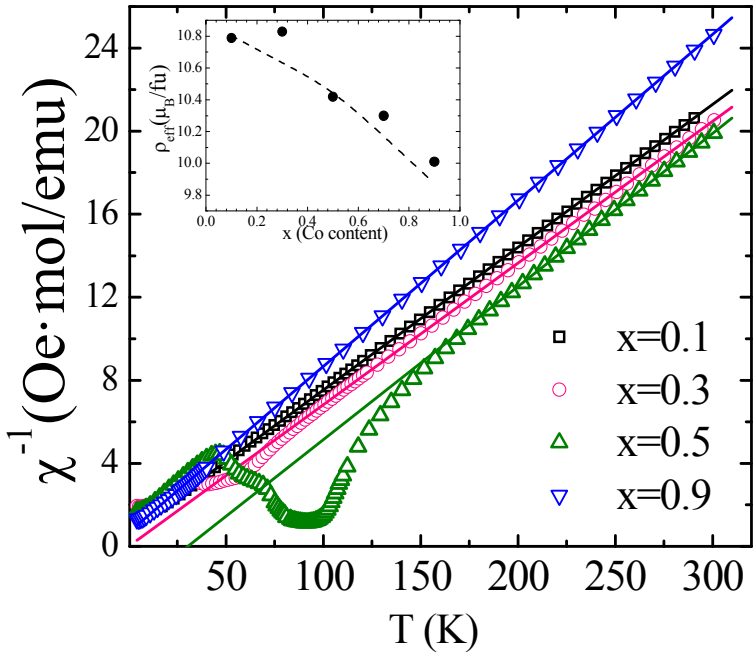

Fig. 5. Temperature evolution of the inverse of DC susceptibility (points) and fit to a Curie-Weiss law at high temperatures (lines). The applied magnetic field is 0.5 T. Inset: effective paramagnetic moments (ρ_{eff}) per unit formula, obtained from the fits. The dashed line represents the calculated ρ_{eff} considering a charge disproportionation model.

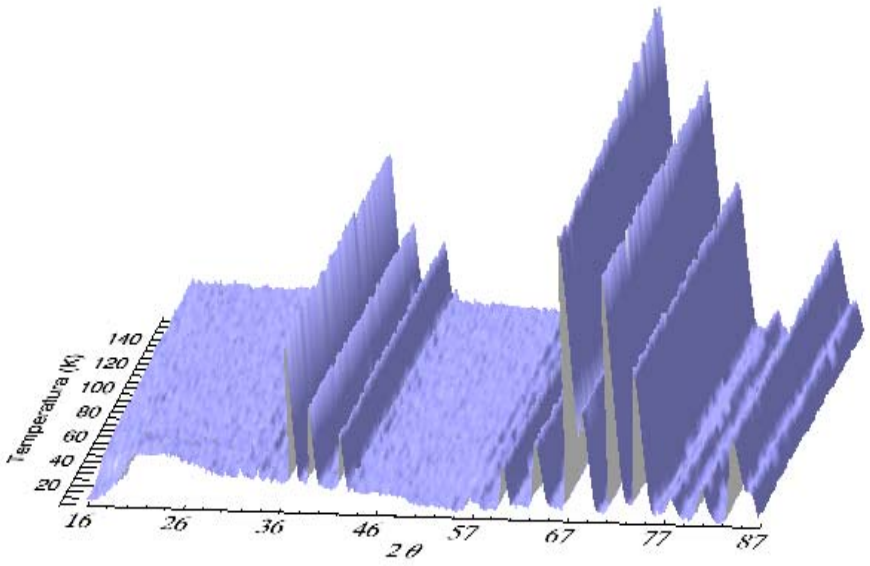

Fig. 6. Neutron thermodiffractogram for $TbMn_{0.9}Co_{0.1}O_3$ between 180 K and 2 K.

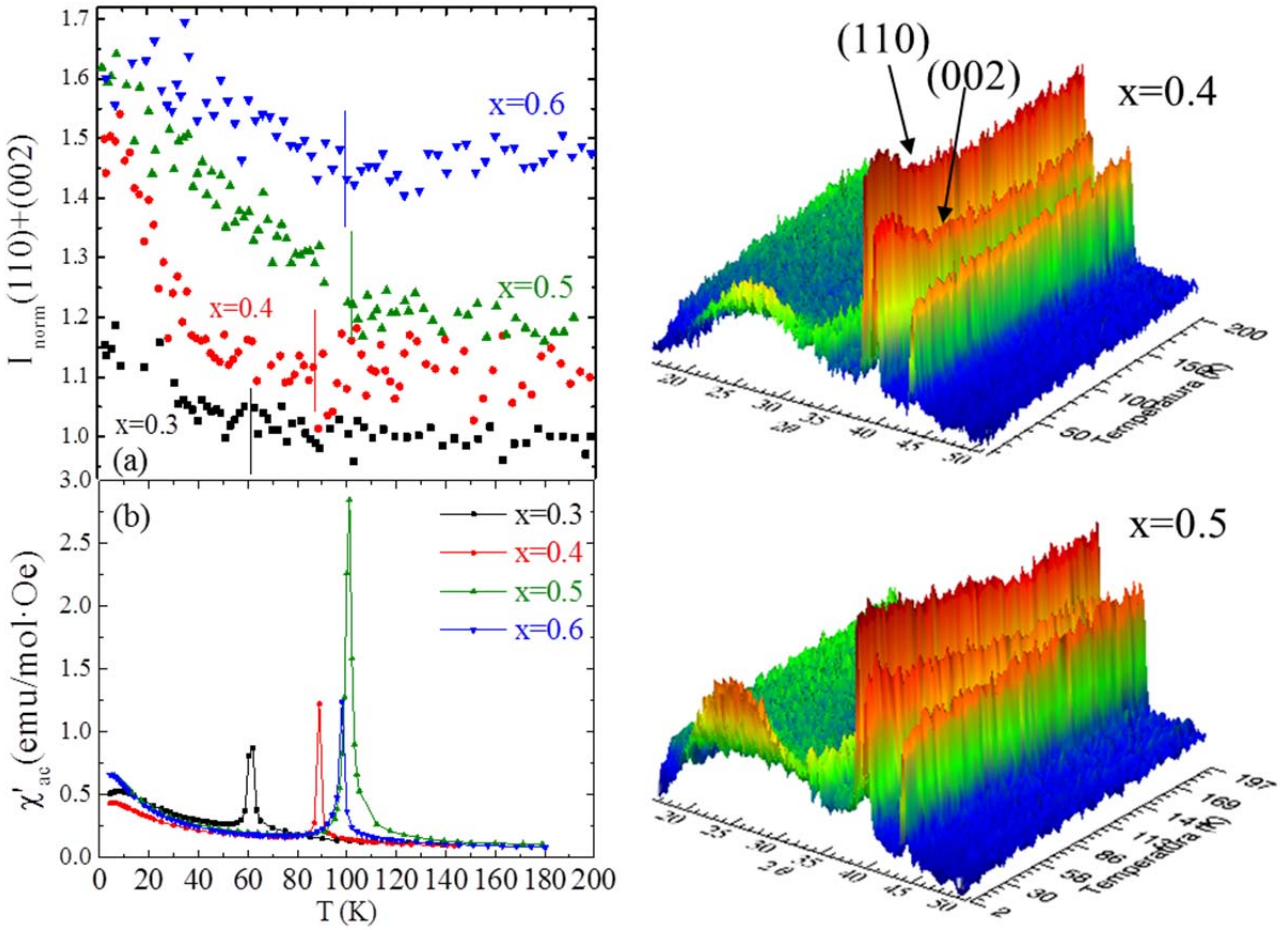

Fig 7. (a) Temperature evolution of the sum of integrated intensities corresponding to (110) and (002) reflections (normalized to its value at 200 K and then *y*-shifted) for x=0.3, 0.4, 0.5 and 0.6. Right panel: low angle part of the thermodiffractograms corresponding to x=0.4 and 0.5 samples, measured with λ=2.52 Å. (b) Real part of ac susceptibility for x=0.3, 0.4, 0.5 and 0.6 samples as a function of temperature, being h_0=4 Oe and ν=117 Hz.

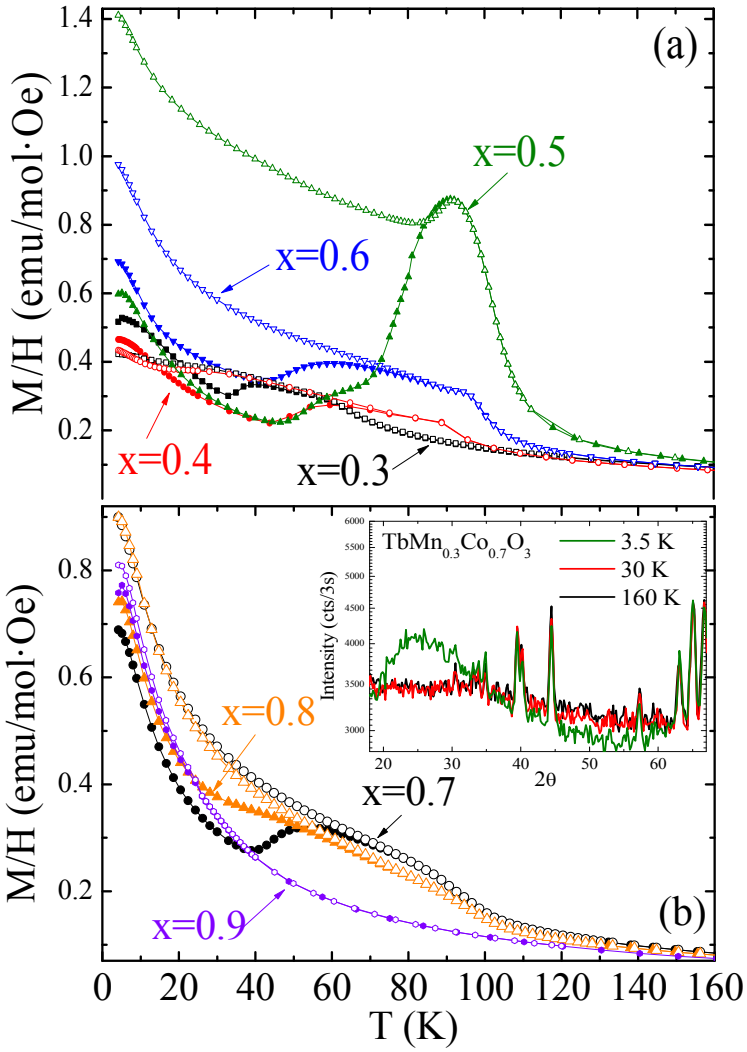

Fig. 8. Zero field cooled (ZFC, filled symbols) and field cooled (FC, open symbols) DC molar susceptibility (M/H) as a function of temperature, under $\mu_0 H$=0.5 T of TbMn1-xCoxO3 for (a) 0.3≤x≤0.6 and (b) 0.7≤x≤0.9. Inset: Neutron diffraction patterns measured at three different (3.5K, 30 K and 160 K) for $TbMn_{0.3}Co_{0.7}O_3$ sample, λ=2.52 Å.

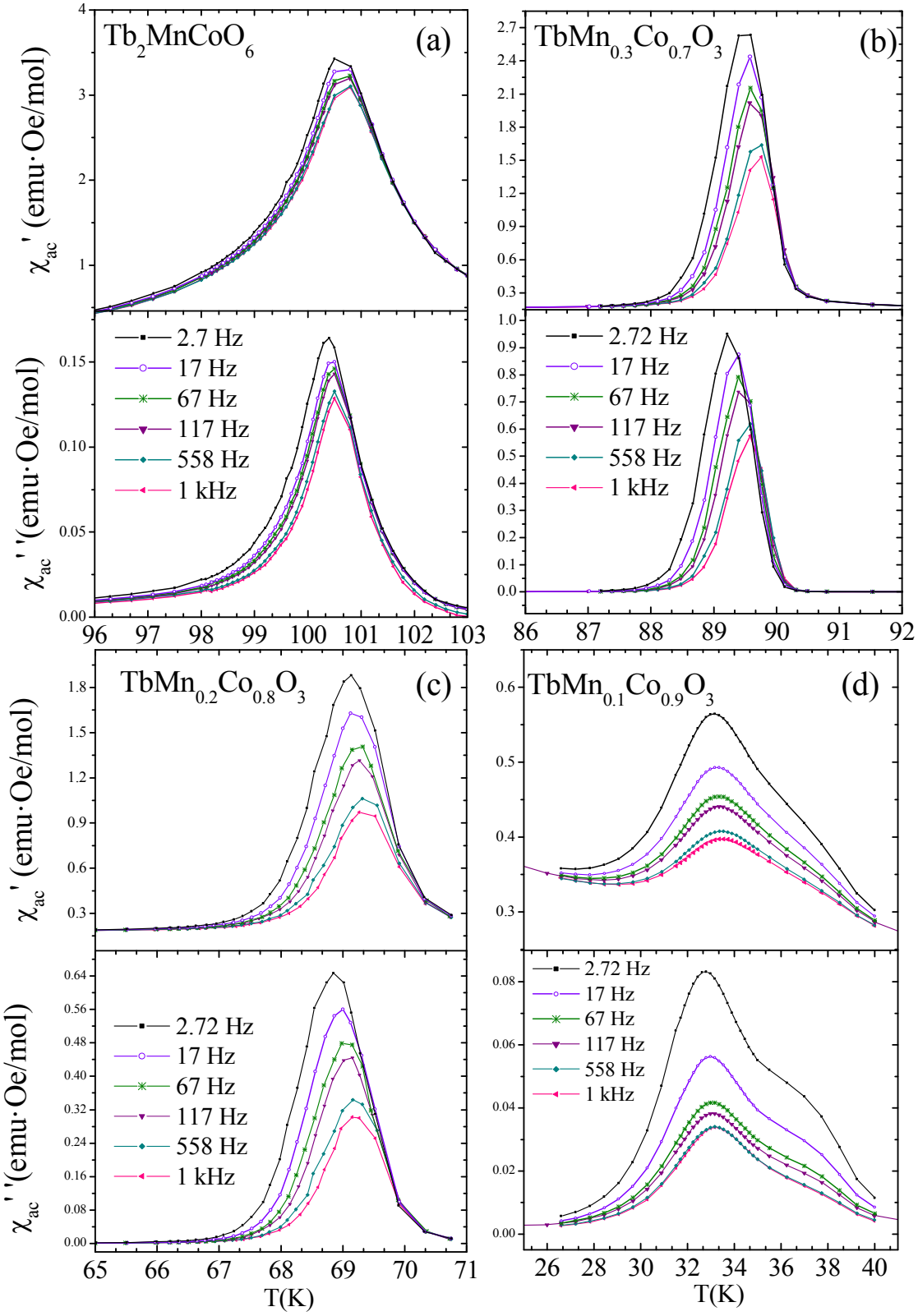

Fig. 9. Temperature dependence of ac susceptibility for x=0.5, 0.7, 0.8 and 0.9 samples at six different frequencies of the magnetic field applied (h_0=4Oe).